DOI: 10.31276/VJSTE.2025.0011

Novel naphthalene-tetrazole butanamide derivatives: synthesis and evaluation of acetylcholinesterase inhibitory activity

Nguyen Viet Hung[1, 2], Nguyen Anh Chi[1], Hoang Tran[1], Tiep K. Nguyen[1], Van-Hai Hoang[3], Tran Thi Thu Hien[4], Le Minh Dong[5], Phuong-Thao Tran[1*]

[1]Hanoi University of Pharmacy, 13-15 Le Thanh Tong Street, Cua Nam Ward, Hanoi, Vietnam
[2]Hanoi University of Mining and Geology, 18 Vien Street, Dong Ngac Ward, Hanoi, Vietnam
[3]Faculty of Pharmacy, Phenikaa University, Nguyen Trac Street, Duong Noi Ward, Hanoi, Vietnam
[4]Vietnam University of Traditional Medicine, 2 Tran Phu Street, Dai Mo Ward, Hanoi, Vietnam
[5]Military Technical Academy, 236 Hoang Quoc Viet Street, Nghia Do Ward, Hanoi, Vietnam

Received 11 March 2025; revised 12 August 2025; accepted 25 August 2025

Abstract:

Acetylcholinesterase (AChE) inhibitors constitute a well-established class of therapeutic agents that provide symptomatic relief in Alzheimer's disease, underscoring the continued importance of developing new compounds with improved efficacy and safety profiles. In this context, five novel derivatives bearing the 4-(5-(naphthalene-2-yl)-2*H*-tetrazol-2-yl)-*N*-phenylbutanamide scaffold were synthesised through four known reactions: [3+2] cycloaddition, *N*-alkylation, saponification, and amidation. The purity of the compounds was confirmed by melting point analysis and thin-layer chromatography (TLC). Structural characterisation was achieved using infrared spectroscopy (IR), high-resolution mass spectrometry (HRMS), and proton and carbon nuclear magnetic resonance spectroscopy (^{1}H-NMR and ^{13}C-NMR). The acetylcholinesterase inhibitory activity of the synthesised compounds was evaluated at five concentrations to determine their IC_{50} values. Compound IVa exhibited the highest inhibitory potency, with an IC_{50} of 467.82±10.77 μM. In addition, the inhibitory potential of the compounds was analysed in relation to their physicochemical properties, including drug-likeness and blood-brain barrier permeability, with none violating Lipinski's rule. Molecular docking studies further revealed that the naphthalene-containing framework demonstrated strong predicted binding affinity to AChE, which may contribute to the observed inhibitory activity. These findings provide novel and valuable structural insights for the development of AChE inhibitor derivatives as potential therapeutic strategies for Alzheimer's disease.

Keywords: **acetylcholinesterase inhibitors, Alzheimer's disease, naphthalene.**

Classification numbers**: 2.2, 3.3**

1. Introduction

As reported by the World Health Organization, Alzheimer's disease (AD) is a neurodegenerative disorder that causes dementia with a significant annual increase in prevalence [1]. In Vietnam, this figure is projected to surge to 1.2 million by 2030, posing considerable challenges to healthcare and social systems in providing care, treatment, and support services, particularly for the elderly population aged 65 and older [2, 3]. Despite numerous efforts to elucidate the pathophysiological mechanisms of Alzheimer's disease, the condition remains not fully understood, and no effective treatment is available to prevent or reverse the disease [4]. Over recent decades, many treatment approaches for Alzheimer's disease have been explored, among which inhibitors of the cholinergic system have shown promising results in alleviating symptoms and hold potential as a basis for a cure in the future [5-8].

The cholinergic hypothesis posits that AD is strongly associated with the activity of the enzyme acetylcholinesterase (AChE) [9, 10]. This enzyme hydrolyses acetylcholine (ACh), an important neurotransmitter that is deficient in patients with AD [11]. Furthermore, the AChE can interact with developing amyloid fibres, forming an AChE - amyloid complex that enhances the synthesis of neurotoxic amyloid-beta (Aβ) peptides [12]. Currently, the FDA has approved three symptomatic treatments based on the cholinergic hypothesis: donepezil, galantamine, and rivastigmine. However, these drugs are associated with significant side effects [5, 6, 13]. Hence, more effort is needed to develop more AChE inhibitors remains an important research priority.

AChE consists of three main structural regions: the catalytic active site (CAS), the catalytic gorge, and the peripheral anionic site (PAS) (Fig. 1A) [14]. The CAS, located at the bottom of the enzyme, is where ACh is hydrolysed, involving key residues such as Ser203, His447, and Glu334 (hAChE). The catalytic gorge is a narrow channel that directs ACh towards the active site, while aromatic residues provide a favourable environment for interaction. The PAS, situated outside the CAS, stabilises and orients ACh before it enters the active site, thereby assisting in

[*]Corresponding author: Email: thaotp@hup.edu.vn

substrate recognition [15, 16]. Effective AChE inhibitors therefore require strong binding affinity for both the PAS and CAS regions. The linker length and structure connecting the two binding sites must be carefully designed to enhance binding efficiency and ensure stability of the enzyme–ligand complex.

In 2019, Tarana Umar and colleagues designed and synthesised naphthalene–triazolopyrimidine derivatives that exhibited strong AChE inhibitory activity (Fig. 1B) [17]. In these inhibitors, the naphthyl scaffold played an important role by engaging in π–π stacking interactions with Trp286 and Trp86-key amino acid residues in the AChE binding pocket. Tetrazoles and their derivatives (C-5 substituents) are notable for exhibiting physicochemical properties similar to those of carboxylate esters while offering greater stability against drug-metabolising enzymes, making them promising candidates for competitive inhibition of ACh at AChE receptors [18]. A. Hameed, et al. (2016) reported that the tetrazole scaffold shows potential for AChE and BChE inhibition [19].

Building on the established structure of the AChE active site, the structure–activity relationships of AChE inhibitors, and the potential biological effects of the naphthalene ring, we synthesised five novel compounds bearing the 4-(5-(naphthalene-2-yl)-2H-tetrazol-2-yl)-N-phenylbutanamide scaffold and evaluated their biological activity against AChE (Fig. 1C). The synthesised compounds were tested for purity, structurally characterised, and assessed for drug-like properties to identify promising AChE inhibitors for further investigation in the treatment of AD.

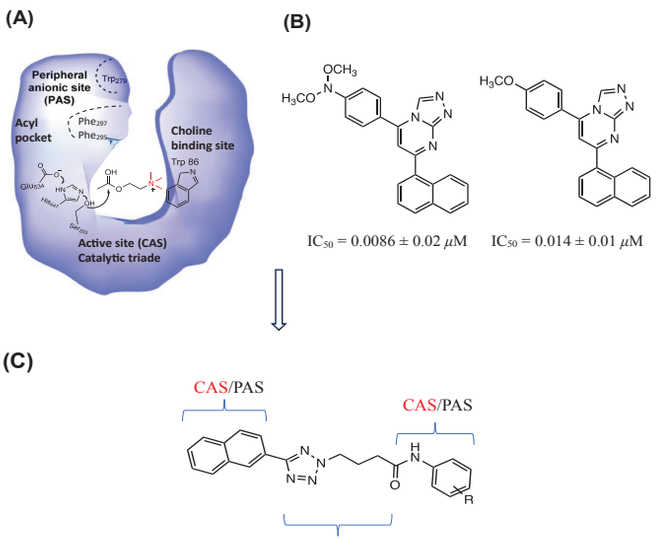

Fig. 1. (A) Illustration of the AChE active site structure. (B) Structures of known AChE inhibitors bearing a naphthalene scaffold. (C) Structures of the synthesised compounds. IVa. R=H; IVb. R=2-Cl; IVc. R=3-Cl; IVd. R=4-Cl; IVe. R=4-Br.

2. Materials and methods

2.1. Chemistry

Reagents were obtained from both national and international suppliers (Merck, Sigma-Aldrich) and used without further purification. Solvents were sourced from Merck (Germany), Sigma-Aldrich, Fisher (USA), as well as suppliers in China and South Korea. The progress of the reactions was monitored using thin-layer chromatography (TLC) on Merck Kieselgel 60F_{254} plates, with compounds visualised under UV light at 254 nm.

The designed compounds (**Iva-e**), bearing the 4-(5-(naphthalene-2-yl)-2*H*-tetrazol-2-yl)-*N*-phenylbutanamide scaffold, were synthesised from 2-naphthalene carbonitrile (**I**) according to the procedure outlined in Scheme 1.

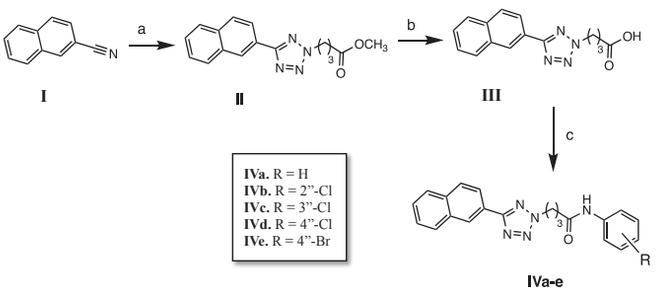

Scheme 1. Synthesis of novel naphthalene derivatives (**IVa-e**). Reagents and conditions: (**a**) i) NaN_3, $ZnCl_2$, DMF, reflux, 8h, ii) methyl-4-chlorobutanoate, 60°C, 2 h; (**b**) i) NaOH, MeOH, rt, 2h, ii) HCl; (**c**) aniline derivatives, HOBt, EDC. HCl, DMF, 60°C, 8 h.

The intermediate compound, methyl 5-(5-(naphthalene-2-yl)-2*H*-tetrazol-2-yl)butanoate (**II**), was synthesised via two sequential reactions: a [3+2] cycloaddition and N-alkylation. Specifically, 2-naphthalene carbonitrile (1.0 equiv.) was dissolved in 5 ml of *N*,*N*-dimethylformamide (DMF) in a 100 ml glass round-bottom flask, followed by the addition of sodium azide (NaN_3, 1.5 equiv.) and zinc chloride ($ZnCl_2$, 0.1 equiv.). The reaction mixture was refluxed for 8 h, then cooled to room temperature before adding methyl 4-chlorobutanoate (1.5 equiv.). The reaction was subsequently heated to 60°C and maintained for 2 h. Upon completion, the mixture was cooled to room temperature, and a saturated sodium carbonate (Na_2CO_3) solution was added to precipitate Zn^{2+}, followed by filtration. The filtrate was extracted with ethyl acetate (EA), and the organic phase was collected and dried over anhydrous sodium sulfate (Na_2SO_4). The solvent was removed under reduced pressure using a rotary evaporator. The resulting residue was purified via silica gel column chromatography with an EA:*n*-hexane (1:3) mobile phase, yielding two isomers, **N1** and **N2**. The **N2** isomer was selected for subsequent reactions.

The ester group of compound **II** was hydrolysed in MeOH using NaOH (aq, 3.0 equiv.) at room temperature for 2 h. The reaction mixture was then adjusted to pH 1-2 using concentrated HCl and evaporated under reduced pressure, yielding acid **III** along with sodium chloride (NaCl). Acid **III** was subsequently purified using a mixture of MeOH:dichloromethane (DCM) (5% DCM) to remove residual salt.

Amide compound **IVa** was synthesised via a one-pot amide coupling reaction. Acid **III** was dissolved in DMF, followed by the addition of hydroxybenzotriazole (HOBt, 1.2 equiv.), *N*-(3-dimethylaminopropyl)-*N*′-ethylcarbodiimide hydrochloride

(EDC·HCl, 1.2 equiv.), aniline (1.2 equiv.), and a minimal amount of DCM. The reaction mixture was stirred and refluxed at 60°C for 8 h. After solvent evaporation, the mixture was neutralised with saturated $NaHCO_3$ solution, then extracted with EA and water to remove water-soluble impurities. The product was purified by silica gel column chromatography using an EA:*n*-hexane mobile phase, yielding compound **IVa** as a solid. Compounds **IVb–IVe** were synthesised from intermediate **III** following the same procedure, using aniline derivatives (1.2 equiv.) as starting materials.

The final product **IVb** was synthesised using a procedure similar to that of **IVa** with 2-chloroaniline (1.2 equiv.) as the starting material.

The final product **IVc** was synthesised using a procedure similar to that of **IVa** with 3-chloroaniline (1.2 equiv.) as the starting material.

The final product **IVd** was synthesised using a procedure similar to that of **IVa** with 4-chloroaniline (1.2 equiv.) as the starting material.

The final product **IVe** was synthesised using a procedure similar to that of **IVa** with 4-bromoaniline (1.2 equiv.) as the starting material.

Melting points of the obtained compounds were measured using an Electrothermal digital thermoelectric melting point apparatus. Nuclear magnetic resonance spectra were measured on a Bruker AC-500 MHz spectrometer at 500 MHz for ^{1}H-NMR and 125 MHz for ^{13}C-NMR, with trichloromethane ($CDCl_3$). Tetramethylsilane (TMS) was used as an internal standard. Mass spectra were recorded using an Agilent 6530 Accurate-Mass QTOF LC/MS (United States) with electrospray ionisation (ESI).

2.2. AChE inhibitory activity

SPL 96-well plates (Korea), 1000 μl and 200 μl tips (AHL, Germany), micropipettes 1000 μl and 200 μl (Nichiryo, Japan); AChE enzyme (Sigma-Aldrich, USA), acetylthiocholine iodide (ATCI, Sigma-Aldrich, USA), 5,5′-dithiobis(2-nitrobenzoic acid) (DTNB, TCI, Japan), and galantamine hydrobromide (TCI, Japan) were used in the experiment to evaluate the AChE inhibitory ability of the synthesised compounds by the spectrophotometric method of G.L. Ellman, et al. (1961) [20] with slight modification [21]. AChE inhibition was evaluated using a Varioskan Lux 96-well plate reader. A reaction mixture containing 20 μl of different concentrations of test solutions in phosphate buffer pH 8.0, 20 μl of 19.2 mM DTNB solution, 20 μl of 19.2 mM ATCI solution, and 20 μl of 0.25 IU/ml AChE solution was prepared, with phosphate buffer pH 8.0 added to a final volume of 200 μl. The mixture was incubated at 25°C for 30 minutes, then the absorbance was measured at a wavelength of 412 nm. Each substance was tested for AChE inhibitory activity at five concentrations: 256 μM, 128 μM, 64 μM, 32 μM, and 16 μM. Each test was repeated independently three times.

The percentage (%) of AChE inhibition of the substances at the tested concentrations was calculated using the following formula:

% inhibition = [1- (test sample - blank)/(control- blank)] x 100%

in which: Blank: ATCI, DTNB in pH 8.0 buffer solution

Control: ATCI, DTNB and enzyme in pH 8.0 buffer

Test sample: test substance (or galantamine hydrobromide control), ATCI, DTNB and enzyme in pH 8.0 buffer solution

The data analyses were conducted using Microsoft Excel (Microsoft Corp., Redmond, WA, USA), and the results are presented as mean ± SD. The AChE inhibitory activity of each sample was quantified by the IC_{50} value, representing the micromolar concentration required to inhibit substrate hydrolysis (ATCI) by 50%, as calculated using TableCurve 2D v4 software.

2.3. Molecular docking simulations

The five synthesised compounds were docked into AChE using AutoDock Vina to determine their binding poses and affinities. The three-dimensional structure of human AChE (PDB ID: 4EY6) was obtained from the Protein Data Bank [21]. AutoDock Tools was used to prepare and parameterise both the receptor and ligands. The docking grid was centred at the native ligand's centre of mass, with dimensions set to 25 × 25 × 25 Å^3. The maximum energy difference among docking modes was 6 kcal·mol^{-1}. The binding conformation with the lowest free energy was visualised using BIOVIA Discovery Studio 2025 Client.

2.4. Physicochemical property studies

The SwissADME platform [22] and BOILED-Egg permeation method [23] was used to assess the physicochemical properties and drug-likeness predictions of synthesised compounds. A potential AChE inhibitor should meet the criteria outlined by Lipinski's Rule of Five [24].

3. Results and discussion

3.1. Chemistry

The five target compounds were synthesised according to Scheme 1. Their purity was verified by measuring melting points and performing TLC, while their structures were confirmed using HRMS and NMR spectroscopy. Detailed information on these spectra is provided below.

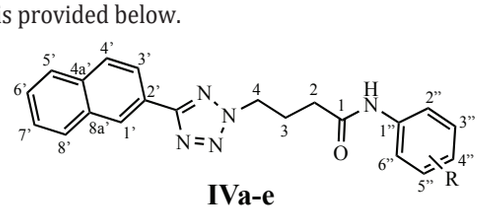

IVa-e

4-(5-(naphthalene-2-yl)-2*H*-tetrazole-2-yl)-*N*-phenylbutanamide (**IVa**). Off white solid, yield: 41%. mp: 185.3 - 187.7°C, R_f = 0.50 (EA: *n*-hexane = 1:1). ^{1}H-NMR (500 MHz, $CDCl_3$, ppm): δ 8.58 (s, 1H, H1'), 8.11 (d, J = 8.5 Hz, 1H, H3'), 7.83 (dd, J =

10.0 Hz, 2H, H4', H8'), 7.80 (d, *J* = 7.7 Hz, 1H, H5'), 7.49-7.44 (m, 4H, H6', H7', H2'', H6''), 7.24 (t, *J* = 8.0 Hz, 2H, H3'', H5''), 7.03 (t, *J* = 7.5, 1H, H4''), 4.75 (t, *J* = 6.2 Hz, 2H, H4), 2.43 (quint, *J* = 6.6 Hz, 2H, H3), 2.37 (t, *J* = 6.8 Hz, 2H, H2). ^{13}H-NMR (125 MHz, $CDCl_3$, ppm): δ 169.4 (C=O), 165.4 (N=C-N), 137.7 (C1''), 134.3 (C4a'), 133.2 (C8a'), 129.1 (C2'), 128.8 (C4'), 128.7(C8'), 127.9 (C3'', C5''), 127.2 (C5'), 126.8 (C7'), 126.7 (C6'), 124.5 (C1', C3'), 123.8 (C4''), 119.9 (C2'', C6''), 52.2 (C4), 33.6 (C2), 25.1 (C3). HR-MS (ESI) m/z calculated for $C_{21}H_{20}N_5O^+$ ($[M+H]^+$) = 358.1662, found 358.1652.

N-(2-chlorophenyl)-4-(5-(naphthalene-2-yl)-2*H*-tetrazol-2-yl)butanamide (**IVb**). Off white solid, yield: 38%. mp: 193.4 - 196.4 °C , R_f=0.55 (EA: *n*-hexane=1:1). ^{1}H-NMR (500 MHz, $CDCl_3$, ppm): *δ* 8.72 (s, 1H, H1'), 8.40 (d, *J*=8.0 Hz, 1H, H3''), 8.25 (dd, *J*=8.5 Hz, 1H, H3'), 7.98 (dd, *J*=8.0 Hz, 2H, H4',H8'), 7.91 (t, *J*=9.5 Hz, 1H, H5''), 7.76 (s, 1H, NH-CO), 7.58 (m, 2H, H6', H7'), 7.39 (dd, *J* = 8.0 Hz, H6''), 7.31 (t, *J*=8.3 Hz, 1H, H5''), 7.08 (td, *J*=7.8 Hz, 1H, H4''), 4.89 (t, *J*=6.3 Hz, 2H, H2), 2.62-2.53 (m, 4H, H3, H4). ^{13}H-NMR (125 MHz, $CDCl_3$, ppm): *δ* 169.4 (C=O), 165.5 (N=C-N), 138.8 (C1''), 134.3 (C4a'), 134.2 (C8a'), 133.2 (C3''), 129.1 (C2'), 128.8 (C4'), 128.7 (C8'), 127.9 (C5''), 127.8 (C2''), 127.2 (C5'), 126.7 (C6', C7'), 124.9 (C3'), 124.6 (C1'), 123.9 (C4''), 121.8 (C6''), 52.1 (C4), 33.9 (C2), 25.0 (C3). HR-MS (ESI) m/z calculated for $C_{21}H_{18}ClN_5ONa^+$ ($[M+H]^+$)=414.1092/416.1063, found 414.0870/416.0882.

N-(3-chlorophenyl)-4-(5-(naphthalene-2-yl)-2*H*-tetrazol-2-yl)butanamide (IVc). Off white solid, yield: 36%. mp: 192.4-194.5 °C, R_f=0.46 (EA: *n*-hexane=1:1). ^{1}H-NMR (500 MHz, $CDCl_3$, ppm): *δ* 8.65 (s, 1H, H1'), 8.18 (dd, *J*=8.5 Hz, 1H, H3'), 7.94 (dd, *J*=8.5 Hz, 2H, H4', H8'), 7.88 (d, *J*=7.5 Hz, 1H, H5'), 7.67 (s, 1H, NH-CO), 7.57-7.52 (m, 3H, H6', H7', H2''), 7.35 (d, *J*=10.0 Hz, 1H, H6''), 7.22 (t, *J*=8.0 Hz 1H, H5''), 7.08 (d, *J*=9.0 Hz, 1H, H4''), 4.83 (t, *J*=6.0 Hz, 2H, H4), 2.50 (quint, *J*=6.4 Hz, 2H, H3), 2.44 (t, *J*=6.8 Hz, 2H, H2). ^{13}H-NMR (125 MHz, $CDCl_3$, ppm): *δ* 169.5 (C=O), 165.5 (N=C-N), 138.8 (C1''), 134.8 (C4a'), 134.3 (C8a'), 133.2 (C3''), 130.0 (C2'), 128.9 (C5''), 128.7 (C4'), 127.9 (C8'), 127.3 (C5'), 126.8 (C7'), 126.7 (C6'), 124.5 (C3'), 124.4 (C1'), 123.8 (C4''), 119.9 (C2''), 117.7 (C6''), 52.1 (C4), 33.6 (C2), 25.0 (C3). HR-MS (ESI) m/z calculated for $C_{21}H_{19}ClN_5O^+$ ($[M+H]^+$)=392.1273/394.1243, found 392.1274/394.1261.

N-(4-chlorophenyl)-4-(5-(naphthalene-2-yl)-2*H*-tetrazol-2-yl)butanamide (**IVd**).

Off white solid, yield: 44%. mp: 196.7-198.3°C, , R_f=0.52 (EA: *n*-hexane=1:1). ^{1}H-NMR (500 MHz, $CDCl_3$, ppm): *δ* 8.65 (s, 1H, H1'), 8.18 (d, *J*=8.5 Hz, 1H, H3'), 7.94 (dd, *J*=11.5 Hz, 2H, H4', H8'), 7.88 (d, *J*=7.5 Hz, 1H, H5'), 7.57-7.52 (m, 2H, H6', H7'), 7.49-7.47 (m, 3H, NH-CO, H2'', H6''), 7.27 (d, *J*=9.3 Hz, 2H, H3'', H5''), 4.83 (t, *J*=6.3 Hz, 2H, H4), 2.50 (quint, *J*=6.3 Hz, 2H, H3), 2.44 (t, *J*=7.0 Hz, 2H, H2). ^{13}H-NMR (125 MHz, $CDCl_3$, ppm): *δ* 169.4 (C=O), 165.5 (N=C-N), 136.2 (C1''), 134.3 (C4a'), 133.2 (C8a'), 129.5 (C3'', C5''), 129.1 (C2'), 128.9 (C4'), 128.7 (C8'), 127.9 (C4''), 127.3 (C5'), 126.8 (C7'), 126.7 (C6'), 124.5 (C3'), 123.8 (C1'), 121.1 (C2'', C6''), 52.2 (C4), 33.6 (C2), 25.0 (C3). HR-MS (ESI) m/z calculated for $C_{21}H_{19}ClN_5O^+$ ($[M+H]^+$)=392.1273/394.1243, found 392.1283/394.1266.

N-(4-bromophenyl)-4-(5-(naphthalene-2-yl)-2*H*-tetrazol-2-yl)butanamide (**IVe**).

Off white solid, yield: 37%. mp: 202.4 - 204.7°C , R_f=0.44 (EA: *n*-hexane=1:1). ^{1}H-NMR (500 MHz, $CDCl_3$, ppm): *δ* 8.66 (s, 1H, H1'), 8.19 (d, *J*=8.0 Hz, 1H, H3'), 7.96 (dd, *J*=9.0 Hz, 2H, H4', H8'), 7.89 (d, *J*=7.5 Hz, 1H, H5'), 7.55 (t, *J*=4.8 Hz, 2H, H6', H7'), 7.45-7.41 (m, 4H, H2'', H3'', H5'', H6''), 4.84 (t, *J*=6.3 Hz, 2H, H4), 2.51 (quint, *J*=6.5 Hz, 2H, H3), 2.44 (t, *J*=7.0 Hz, 2H, H2). ^{13}H-NMR (125 MHz, $CDCl_3$, ppm): *δ* 169.4 (C=O), 165.5 (N=C-N), 136.7 (C1''), 134.3 (C4a'), 133.2 (C8a'), 132.0 (C3'', C5''), 128.9 (C2'), 128.7 (C4'), 127.9 (C8'), 127.3 (C5'), 126.8 (C7'), 126.7 (C6'), 124.5 (C3'), 123.8 (C1'), 121.4 (C2'', C6''), 117.1 (C4''), 52.2 (C4), 33.7 (C2), 25.0 (C3). HR-MS (ESI) m/z calculated for $C_{21}H_{19}BrN_5O^+$ ($[M+H]^+$)=436.0767/438.0747, found 436.0770/438.0752.

The spectral analysis results unequivocally confirmed that the structures of the synthesised derivatives aligned with the initial predictions. The ^{1}H-NMR spectra of all compounds exhibited the expected number of proton signals in both the aromatic and methylene regions, confirming structural integrity. The N–H proton signals were inherently weak and difficult to discern, likely due to their high mobility, which facilitates proton exchange or tautomeric equilibrium with the solvent ($CDCl_3$). This feature is also characteristic of the final compound, as it typically appears as a singlet with low intensity and often displays a broad, square-shaped pattern. In this series, the propylene group proton was identified by three signals: the triplet signal of N-CH_2 at δ 4.89-4.75 ppm and the multiplet signal of the remaining methylene protons at δ 2.62-2.37 ppm. These signals were consistent across the synthesised compounds. Likewise, the ^{13}C-NMR spectra validated the presence of the complete set of carbon atoms within the synthesised molecules and confirmed the presence of the C=O group at approximately δ 169.0 ppm and the N=C–N carbon at around δ 165.0 ppm. Furthermore, the mass spectrometry data revealed the molecular ion peak $[M+H]^+$, which corresponded precisely to the calculated molecular weight of the target compounds. Notably, compounds IVb-e bearing chlorine (Cl) or bromine (Br) substituents, due to their naturally occurring isotopes, displayed two characteristic major ion peaks in their mass spectra, further substantiating their molecular composition.

3.2. AChE inhibitory activity

Compounds IVa-e were evaluated for their AChE inhibitory activity at concentrations of 256 μM, 128 μM, 64 μM, 32 μM, and 16 μM, and compared with the positive control, galantamine hydrobromide. The results are expressed as IC_{50} values, as shown in Table 1.

Table 1. The IC_{50} value of five synthesised compounds on the AChE enzyme.

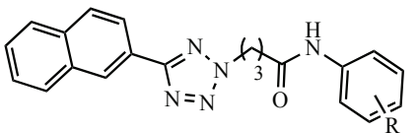

Compounds	R	IC_{50} (μM)
IV-a	H	467.82±10.77
IV-b	2-Cl	>1000
IV-c	3-Cl	>1000
IV-d	4-Cl	707.95±59.34
IV-e	4-Br	530.96±12.74
Positive control	Galantamine hydrobromide: IC_{50}=2.5±0.2 μM	

The IC_{50} values were calculated based on three independent experiments.

The activity test results showed that compound IVa had the lowest IC_{50} value, indicating the best AChE inhibitory activity, followed by compounds IVd and IVe, which demonstrated moderate inhibition with IC_{50} values of 707.95±59.34 μM and 530.96±12.74 μM, respectively. Meanwhile, IVb and IVc did not exhibit AChE inhibitory activity at the tested concentrations.

The results indicated that different substituent groups on the benzene ring affected AChE inhibitory activity. Compounds IVb and IVc, with Cl substituents at the ortho and meta positions, showed poor inhibition (IC_{50}>1000 μM). In contrast, compounds IVd and IVe, with Cl and Br at the para position, exhibited significantly better inhibition, suggesting that this positioning creates more stable interactions. It is evident that the introduction of halogen substituents generally leads to a decrease in activity. This may be attributed to the fact that the core structures of the compounds in this series are already relatively bulky and rigid, so the addition of halogen atoms, especially at the ortho and meta positions, further increases the molecular size, potentially hindering the compounds' ability to access the narrow and confined active site of AChE. The decrease in inhibitory activity may also be due to the electron-withdrawing ability of halogens. However, derivatives bearing other electron-donating or electron-withdrawing substituents still need to be synthesised and evaluated for their biological activity to draw a more definitive conclusion.

3.3. Molecular docking simulation

To gain deeper insights into the interactions between the synthesised compounds and AChE, molecular docking simulations were performed at the enzyme's active site. AutoDock Vina was first validated by docking galantamine into the AChE crystal structure (PDB ID: 4EY6), which yielded an RMSD value of 0.33 Å and a binding energy of –10.4 kcal·mol^{-1} (Table 2), aligning well with its known inhibitory properties. The docking results for the five target compounds showed binding energies ranging from -11.5 to -10.8 kcal·mol^{-1} (Table 2), suggesting a strong affinity for AChE. Notably, compound **IVa** demonstrated the highest binding affinity (-11.5 kcal·mol), supporting its role as the most potent AChE inhibitor in the series.

Table 2. Binding energies of compound IVa-e and galantamine.

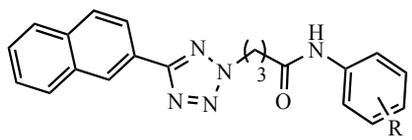

Compounds	R	Binding energy (kcal.mol^{-1})
IV-a	H	-11.5
IV-b	2-Cl	-10.9
IV-c	3-Cl	-10.8
IV-d	4-Cl	-11.0
IV-e	4-Br	-11.1
Galantamine	-10.4	

The docking results of the naphthyl-based derivatives showed higher scores compared with galantamine, which may be attributed to the relatively rigid structure of the naphthyl scaffold. This rigidity likely results in a greater entropy change when these compounds transition from the ground state to the bound state, contributing to better calculated docking scores that correlate with Gibbs free energy.

Interaction analysis (Fig. 2) revealed that the derivatives formed key interactions as predicted, particularly with critical amino acid residues such as Trp86 in the choline-binding site, as well as Phe338, Phe297, and Asp74 within the acyl pocket and the peripheral anionic site (PAS). Notably, the naphthyl scaffold tended to form π–π stacking interactions with Trp86, while the phenyl ring engaged in similar stacking interactions with residues such as Phe338 and Phe297. These interaction patterns are consistent with those observed for galantamine, which also exhibits π–π stacking with Trp86 and interactions with Phe338 and Phe297, suggesting that the synthesised derivatives may share similar binding modes to this reference inhibitor.

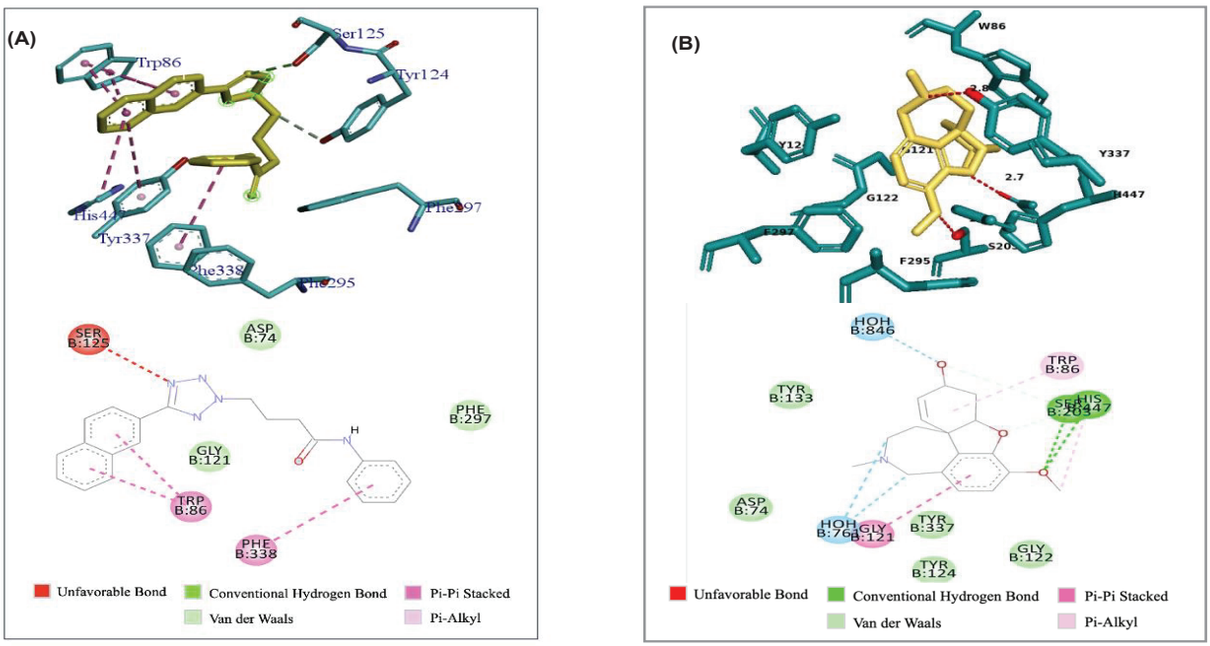

Fig. 2. Predicted binding interations of (A) compound IVa and (B) galantamine in the active site of AChE (PDB ID: 4EY6).

3.4. Physicochemical properties and drug-likeness predictions

The validation of the physicochemical properties of synthesised compounds **IVa-e** was presented in Table 3.

All compounds comply with Lipinski's Rule of Five, indicating favourable drug-like properties and potential for oral bioavailability. The observed increase in lipophilicity due to halogen substitutions, particularly with bromine, may enhance binding affinity; however, it could also negatively impact solubility and metabolic stability. In addition, compounds **IVa–e** were determined to have the ability to cross the blood–brain barrier, as their TPSA and WlogP values fall within the yellow region of the BOILED-Egg diagram. These observations further support the potential of the naphthalene-based compounds in the treatment of Alzheimer's disease (AD).

Table 3. Calculated physicochemical properties of target compounds IVa-e.

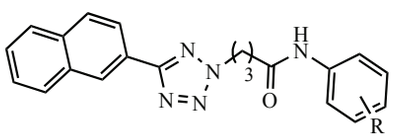

Cpds	R	MW*	MlogP	WlogP	TPSA (Å^2)*	HBD*	HBA*
IVa	H	357.41	2.84	3.72	72.70	1	4
IVb	2-Cl	391.85	3.32	4.37	72.70	1	4
IVc	3-Cl	391.85	3.32	4.37	72.70	1	4
IVd	4-Cl	391.85	3.32	4.37	72.70	1	4
IVe	4-Br	436.30	3.43	4.48	72.70	1	4
RO5**		≤500	≤5			≤5	≤10

*MW: Molecular weight; MlogP: LogP calculated by the Moriguchi method; WlogP: LogP calculated by Wildman and Crippen; TPSA: Topological Polar Surface Area; HBD: Hydrogen Bonding Donor; HBA: Hydrogen Bonding Acceptor; **RO5: Lipinski's Rule of Five.

4. Conclusions

In this study, we successfully synthesised five novel aromatic derivatives (**IVa–e**) featuring a 4-(5-(naphthalene-2-yl)-2*H*-tetrazol-2-yl)-*N*-phenylbutanamide scaffold, starting from 2-naphthalene carbonitrile through a three-step reaction. Structural characterisation by HR-MS and NMR spectroscopy confirmed that the synthesised compounds were consistent with their expected chemical structures. Among the five derivatives, IVa exhibited the most potent AChE inhibitory activity. Molecular docking studies further suggested that the compounds were able to establish favourable interactions within the AChE binding site, with key π–π stacking interactions observed between the naphthalene ring and Trp86, which likely contributed to the observed binding affinity. Additional analysis of drug-like properties indicated that all five compounds fulfilled the standard physicochemical requirements for drug-like molecules. Collectively, these findings suggest that the synthesised derivatives possess potential as AChE inhibitors for AD treatment, thereby warranting further investigation. By introducing a novel naphthalene-based scaffold, this work provides a new structural platform for the design and development of future AChE inhibitors targeting Alzheimer's disease.

These findings suggest that the synthesised derivatives have potential as AChE inhibitors for AD treatment, warranting further investigation. By introducing a novel naphthalene-based

scaffold, this work provides a new structural platform for the design of future AChE inhibitors targeting Alzheimer's disease. Future studies should concentrate on synthesising additional naphthalene derivatives particularly those incorporating halogen atoms at the 4-position or other electron-withdrawing groups as well as analogues containing alternative core scaffolds. Moreover, extended molecular docking simulations and more extensive biological evaluations will be essential to identify derivatives with improved inhibitory potency and to provide guidance for rational structure-based optimisation in the search for promising anti-Alzheimer's drug candidates.

CRediT author statement

Nguyen Viet Hung: Methodology, Investigation, Validation, Writing - Reviewing and Editing; Nguyen Anh Chi: Software, Methodology, Investigation, Validation, Simulation studies, Writing - Reviewing and Editing; Hoang Tran: Software, Simulation studies, Visualisation, Data curation, Writing - Reviewing and Editing; Tiep K. Nguyen: Methodology, Bio-assay experiments, Validation, Writing - Reviewing and Editing; Van-Hai Hoang: Investigation, Validation, Writing - Reviewing and Editing; Tran Thi Thu Hien: Investigation, Validation, Writing - Reviewing and Editing; Le Minh Dong: Investigation, Validation, Writing - Reviewing and Editing; Phuong-Thao Tran: Conceptualisation, Methodology, Investigation, Data curation, Visualisation, Writing - Original draft preparation, Writing - Reviewing and Editing.

ACKNOWLEDGMENTS

This research is funded by project number T25-16 of Hanoi University of Mining and Geology, Vietnam; and Vingroup Innovation Fund (VINIF) under Project code VINIF.2022.DA00061.

COMPETING INTERESTS

The authors declare that there is no conflict of interest regarding the publication of this article.

REFERENCES

[1] R. Cataldi, P.S. Sachdev, N. Chowdhary, et al. (2023), "A WHO blueprint for action to reshape dementia research", *Nat. Aging*, **3(5)**, pp.469-471, DOI: 10.1038/s43587-023-00381-6.

[2] T.A. Nguyen, T. Pham, T.H. Dang, et al. (2020), "Towards the development of Vietnam's national dementia plan-the first step of action", *Australas J. Ageing*, **39(2)**, pp.137-141, DOI: 10.1111/ajag.12755.

[3] E. Nichols, T. Vos (2021), "The estimation of the global prevalence of dementia from 1990-2019 and forecasted prevalence through 2050: An analysis for the Global Burden of Disease (GBD) study 2019", *Alzheimer's & Dementia*, **17**, DOI: 10.1002/alz.051496.

[4] B.J.J. Gaugler, T. Johnson, et al. (2024), "Alzheimer's disease facts and figures", *Alzheimers Dement*, **20(5)**, pp.3708-3821, DOI: 10.1002/alz.13809.

[5] L.K. Huang, Y.C. Kuan, H.W. Lin, et al. (2023), "Clinical trials of new drugs for Alzheimer disease: a 2020-2023 update", *J. Biomed Sci.*, **30(1)**, DOI: 10.1186/s12929-023-00976-6.

[6] S.L. Motebennur, B.P. Nandeshwarappa, M.S. Katagi (2023), "Candidates for the treatment of Alzheimer's disease: New findings from 2021 and 2022", *Drugs and Drug Candidates*, **2(3)**, pp.571-590, DOI: 10.3390/ddc2030030.

[7] M.A.A. Orabi, A.H. Hasan, S.F. AbouZid, et al. (2023), "Nutritional, antioxidant, antimicrobial, and anticholinesterase properties of phyllanthus emblica: A study supported by spectroscopic and computational investigations", *Metabolites*, **13(9)**, DOI: 10.3390/metabo13091013.

[8] A.H. Hasan, S.I. Amran, F.H.S. Hussain, et al. (2019), "Molecular docking and recent advances in the design and development of cholinesterase inhibitor scaffolds: Coumarin hybrids", *Chemistry Select.*, **4(48)**, pp.14140-14156, DOI: 10.1002/slct.201903607.

[9] A. Majdi, S.S. Eteghad, S.R. Aghsan, et al. (2020), "Amyloid-β, tau, and the cholinergic system in Alzheimer's disease: Seeking direction in a tangle of clues", *Rev. Neurosci.*, **31(4)**, pp.391-413, DOI: 10.1515/revneuro-2019-0089.

[10] K. Gajendra, G.K. Pratap, D.V. Poornima, et al. (2024), "Natural acetylcholinesterase inhibitors: A multi-targeted therapeutic potential in Alzheimer's disease", *European Journal of Medicinal Chemistry Reports*, **11**, DOI: 10.1016/j.ejmcr.2024.100154.

[11] Z.R. Chen, J.B. Huang, S.L. Yang, et al. (2022), "Role of cholinergic signaling in Alzheimer's disease", *Molecules*, **27(6)**, DOI: 10.3390/molecules27061816.

[12] H. Hampel, M. Mesulam, A.C. Cuello, et al. (2018), "The cholinergic system in the pathophysiology and treatment of Alzheimer's disease", *Brain*, **141(7)**, pp.1917-1933, DOI: 10.1093/brain/awy132.

[13] J. Zhang, Y. Zhang, J. Wang, et al. (2024), "Recent advances in Alzheimer's disease: Mechanisms, clinical trials and new drug development strategies", *Signal Transduct Target Ther.*, **9(211)**, DOI: 10.1038/s41392-024-01911-3.

[14] K.V. Dileep, K. Ihara, C.T. Mishima, et al. (2022), "Crystal structure of human acetylcholinesterase in complex with tacrine: Implications for drug discovery", *International Journal of Biological Macromolecules*, **210**, pp.172-181, DOI: 10.1016/j.ijbiomac.2022.05.009.

[15] J.L. Sussman, M. Harel, F. Frolow, et al. (1991), "Atomic structure of acetylcholinesterase from Torpedo californica: A prototypic acetylcholine-binding protein", *Science*, **253(5022)**, pp.872-879, DOI: 10.1126/science.1678899.

[16] H. Dvir, I. Silman, M. Harel, et al. (2010), "Acetylcholinesterase: From 3D structure to function", *Chem. Biol. Interact.*, **187(1-3)**, pp.10-22, DOI: 10.1016/j.cbi.2010.01.042.

[17] T. Umar, S. Gusain, M.K. Raza, et al. (2019), "Naphthalene-triazolopyrimidine hybrid compounds as potential multifunctional anti-Alzheimer's agents", *Bioorg. Med. Chem.*, **27(14)**, pp.3156-3166, DOI: 10.1016/j.bmc.2019.06.004.

[18] N. Kaushik, N. Kumar, A. Kumar, et al. (2018), "Tetrazoles: Synthesis and biological activity", *Immunology, Endocrine & Metabolic Agents in Medicinal Chemistry*, **18(1)**, pp.3-21, DOI: 10.2174/1871522218666180525100850.

[19] A. Hameed, S.T. Zehra, S. Abbas, et al. (2016), "One-pot synthesis of tetrazole-1,2,5,6-tetrahydronicotinonitriles and cholinesterase inhibition: Probing the plausible reaction mechanism via computational studies", *Bioorg. Chem.*, **65**, pp.38-47, DOI: 10.1016/j.bioorg.2016.01.004.

[20] G.L. Ellman, K.D. Courtney, V. Andres, et al. (1961), "A new and rapid colorimetric determination of acetylcholinesterase activity", *Biochem. Pharmacol.*, **7**, pp.88-95, DOI: 10.1016/0006-2952(61)90145-9.

[21] T.P. Thao, D.H. Hoang, D.T. Hoang, et al. (2024), "Structures and acetylcholinesterase inhibition abilities of some derivatives bearing (pyridin-2-yl) tetrazole scaffold", *VNU Journal of Science: Natural Sciences and Technology*, **40 (2)**, DOI: 10.25073/2588-1140/vnunst.5641.

[22] A. Daina, O. Michielin, V. Zoete (2017), "Swiss ADME: A free web tool to evaluate pharmacokinetics, drug-likeness and medicinal chemistry friendliness of small molecules", *Sci. Rep.*, **7**, DOI: 10.1038/srep42717.

[23] A. Daina, V. Zoete (2016), "A BOILED-Egg to predict gastrointestinal absorption and brain penetration of small molecules", *ChemMedChem.*, **11(11)**, pp.1117-1121, DOI: 10.1002/cmdc.201600182.

[24] C.A. Lipinski (2016), "Rule of five in 2015 and beyond: Target and ligand structural limitations, ligand chemistry structure and drug discovery project decisions", *Adv. Drug. Deliv. Rev.*, **101**, pp.34-41, DOI: 10.1016/j.addr.2016.04.029.